New Journal of Physics
The open access journal at the forefront of physics
Deutsche Physikalische Gesellschaft DPG
IOP Institute of Physics

PAPER • OPEN ACCESS

Nondegenerate two-way edge channels of plasmons in networks

To cite this article: Ken-ichi Sasaki 2023 *New J. Phys.* **25** 083005

IOP Publishing New J. Phys. 25 (2023) 083005 https://doi.org/10.1088/1367-2630/ace7ef

New Journal of Physics

The open access journal at the forefront of physics

Deutsche Physikalische Gesellschaft DPG
IOP Institute of Physics

Published in partnership with: Deutsche Physikalische Gesellschaft and the Institute of Physics

RECEIVED
8 February 2023

REVISED
11 July 2023

ACCEPTED FOR PUBLICATION
17 July 2023

PUBLISHED
2 August 2023

PAPER

Nondegenerate two-way edge channels of plasmons in networks

Ken-ichi Sasaki

NTT Research Center for Theoretical Quantum Physics and NTT Basic Research Laboratories, NTT Corporation, 3-1 Morinosato Wakamiya, Atsugi, Kanagawa 243-0198, Japan

E-mail: kenichi.sasaki.af@hco.ntt.co.jp

Keywords: plasmons, quantum Hall effect, edge magnetoplasmons, domain network

Abstract

An effective one-dimensional channel is formed at the periphery of a two-dimensional electron gas by electronic edge states. Robust edge states with suppressed dissipation arise from the Landau quantization in a strong magnetic field, and propagation through an edge channel formed by these states is one-way. In general, two-way edge channels rather than one-way ones have more advantages for applications and are the main topic of topological insulators. However, two-way edge channels of these are degenerate in their energies, which causes backscattering and dissipation. Here, we show that excited states in networks composed of capacitively coupled integer quantum Hall systems exhibit macroscopic two-way edge channels with different energies. Theoretical results are derived on the basis of two known effects; each system has plasmonic excitations known as edge magnetoplasmons, and the chirality of each system is diverted only locally by the capacitive interaction between nearest-neighbor systems. Because of the simplicity of the model, various extensions from regular networks to more complicated higher-dimensional networks are possible. The networks provide an ideal platform to test the functionality of plasmonic one-dimensional edge channels and suggest a dynamical model of fractional Quantum Hall systems.

1. Introduction

Topological insulators necessarily have edge states at their peripheries. The edge states provide unique conducting channels along the edge when the interior of the system is insulating. Because topology guarantees their existence, they are robust against various perturbations [1, 2]. The integer quantum Hall effect of a two-dimensional electron gas in a stationary external magnetic field applied perpendicular to the plane is a prime example of a topological insulator and thus is suitable for examining topologically protected edge states [3]. Excited edge states, which are referred to as edge magnetoplasmons (EMPs), exhibit one-way or chiral propagation that moves in a direction determined by the orientation of the external magnetic field [4–9]. Their dynamics have been investigated from various viewpoints for more than three decades. Two-way edge channels rather than one-way ones have been explored for fractional quantum Hall effect [10–12]. In particular, they have led to the idea of using spin degrees of freedom to make topological insulators with time-reversal symmetry [2, 13]. However, two-way edge channels are degenerate in their energies, which potentially makes their conduction properties susceptible to perturbations that one-way channels would be immune.

Interestingly, it is possible to simulate two-way edge channels by separating a single integer quantum Hall system into two systems using microfabrication techniques [14]. Counter propagating channels appear in the coupled region of two quantum Hall domains, and EMPs in the two systems can interact with each other through the inter-domain Coulomb interaction. It is known and as we will explain in detail below that chiral propagation of counter propagating edge channels is diverted by the capacitive interaction between them, which is fundamentally related to intriguing phenomena such as the emergence of non-chiral Tomonaga–Luttinger (TL) liquid and charge-density fractionalization. When a single quantum Hall system is separated into many domains, the signal of broken chirality should naturally appear in such a domain network.

In a previous paper, [15] we calculated the energy band structures of the domain networks by assuming that the networks were periodic. The band structures exhibit the energy band gap which increases with increasing the inter-domain coupling strength. The existence of the energy gap has the similarity to the fractional quantum Hall effect. Note that to understand fractional quantum Hall effect none edge states are necessary because the effect is of bulk type in the thermodynamic limit without boundaries. The edge states were expected to exist if the network had boundaries (or the networks were considered as plasmonic topological insulators) but could not be shown explicitly. In this paper, we use a numerical approach to show that finite domain networks with boundaries indeed hold the edge states. In addition, we show that macroscopic two-way channels are formed at the periphery of a domain network and that they can have different energy eigenvalues. The appearance of two-way edge channels (in strongly-coupled domain networks) is also analogous to the fractional quantum Hall effect.

2. Charge-density fractionalization

Let us describe the process of charge-density fractionalization in two capacitively coupled domains, [16, 17] which is a good example for illustrating how chirality is broken by the inter-domain Coulomb interaction. Suppose that a wave packet with charge Q is excited by the injection gate (see figure 1(a)). The packet propagates along the periphery of the upper domain according its proper chirality (represented by red arrows) at a certain propagation velocity v and approaches the coupled region. When it reaches the left corner of the coupled region, two packets with $\pm rQ$ are pair-created in the lower domain, where $r \in [0,1]$ is the coupling constant of the two domains that can be increased by decreasing the inter-domain distance. Here, charge is conserved in each domain, because charge transfer between domains is avoided by keeping the distance between the two domains sufficiently large [18]. As shown in figure 1(a), the wave packet with charge $-rQ$ of the lower domain combines with the original packet with charge Q of the upper domain through the attractive Coulomb interaction and propagates to the right slowly with a suppressed propagation velocity,

$$v_c = \frac{1-r}{1+r} v, \tag{1}$$

in the form of a bound state (represented by dashed circle) carrying total charge $(1-r)Q$. Note that the packet with $-rQ$ of the lower domain propagates in the direction opposite to the proper chirality of the lower domain. The attractive interaction of the input packet in the upper domain drags the packet with $-rQ$ of the lower domain, and as a result, the chirality of the lower domain is diverted. Meanwhile, the other packet with charge rQ propagates while maintaining the proper chirality (and propagation velocity) of the lower domain and is detected by Det2.

When the bound state arrives at the right corner of the coupled region, the component with charge Q in the first domain goes toward Det1 with velocity v. On the other hand, the partner with charge $-rQ$ in the second domain becomes free from the attractive force and recovers its proper chirality and starts to propagate to the left. Then, another packets with charge $\pm r^2 Q$ are pair-created in the upper domain. A new composite packet with charge $-r(1-r)Q$ forms, which propagates to the left. Charge fractionalization continues to occur when the new bound state reaches the left corner of the coupled region. The packet with charge $-r^2 Q$ combines with the original packet with charge Q and goes to Det1 as a bound state.

When the two domains merge into a single domain, the r value is given by the strong-coupling limit $r \to 1$. In the limit, the initial packet that reaches the left end of the coupled region effectively goes into the second domain, while the bound state with $\pm Q$ stays there because $v_c \to 0$ in the limit. No signal is expected to arrive at Det1. This is reasonable from the viewpoint of the chirality of a single domain (which corresponds to the vanishing inter-domain distance). Moreover, if charge transfer between the domains is taken into account, the bound state will eventually annihilate by recombination.

3. Method

The time evolution of the wave packet described above can be understood within the theoretical framework of the distributed-element circuit model of EMP transport [19]. The current density of angular frequency ω in the coupled region of domains 1 and 2 is the sum of the right and left moving components, [15]

$$\begin{pmatrix} j_1(x) \\ j_2(x) \end{pmatrix} = \alpha_{\mathrm{R}} \begin{pmatrix} 1 \\ -r \end{pmatrix} \mathrm{e}^{+\mathrm{i}\frac{\omega}{v_c}x} - \alpha_{\mathrm{L}} \begin{pmatrix} -r \\ 1 \end{pmatrix} \mathrm{e}^{-\mathrm{i}\frac{\omega}{v_c}x}, \tag{2}$$

where $\alpha_{R/L}$ is the amplitude of the right/left moving components. The two components structure of equation (2) tells that unless $r=0$, two counter-propagating modes of different domains are coupled and

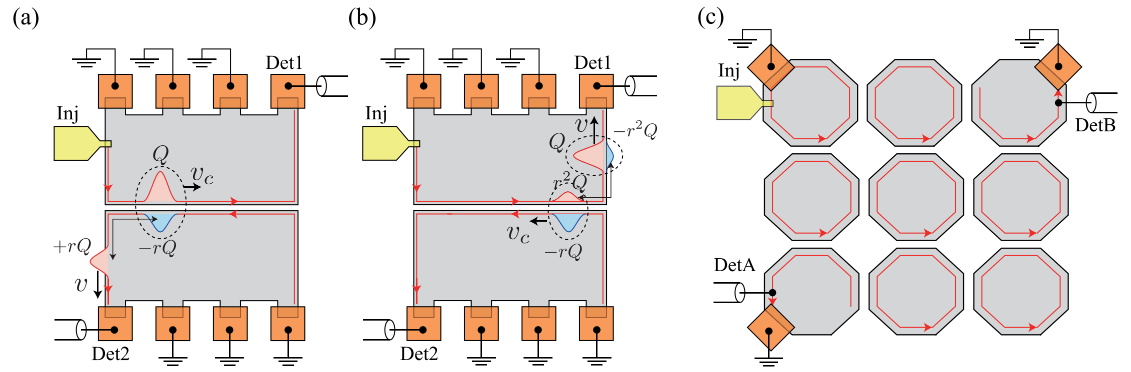

Figure 1. Interacting EMPs in nearest-neighbor domains. (a), (b) Time evolution of a wave packet (with charge Q) excited by the injection gate of the upper domain. (a) When the packet enters into the coupled region, two packets with charge $\pm rQ$ are pair-created in the lower domain at the left corner of the coupled region. A bound state forms through the Coulomb interaction. (b) When the packet of the upper domain leaves the coupled region, two packets with charge $\pm r^2 Q$ are pair-created in the upper domain at the right corner of the coupled region. Two bound states form: one goes to Det1, and the other propagates in the coupled region following the chirality of the lower domain. (c) An example of domain network is shown. The injection gate is attached to the domain at the upper left, and two detectors (DetA and DetB) are attached to investigate the transport properties of the system. The circumferential length of each domain with a regular octagonal shape is $L = 8\ell$, where ℓ denotes the length of a coupled region, which is the same as that of an uncoupled region.

chirality is diverted. By eliminating $\alpha_{\rm R}$ and $\alpha_{\rm L}$ from equation (2), we can relate the current densities at the corners of two capacitively coupled domains in terms of the transfer matrix,

$$\begin{pmatrix} j_1(0) \\ j_1(\ell) \end{pmatrix} = T(\omega) \begin{pmatrix} j_2(0) \\ j_2(\ell) \end{pmatrix}, \tag{3}$$

where ℓ denotes the length of the coupled region,

$$T(\omega) \equiv \begin{pmatrix} 1 & 1 \\ e^{i\frac{\omega}{v_c}\ell} & e^{-i\frac{\omega}{v_c}\ell} \end{pmatrix} \begin{pmatrix} \frac{1}{r} & 0 \\ 0 & r \end{pmatrix} \begin{pmatrix} 1 & 1 \\ e^{i\frac{\omega}{v_c}\ell} & e^{-i\frac{\omega}{v_c}\ell} \end{pmatrix}^{-1} = \frac{1}{-2ir\sin\left(\frac{\omega\ell}{v_c}\right)} \begin{pmatrix} t_\omega & -t_0 \\ t_0 & -t_\omega^* \end{pmatrix}, \tag{4}$$

and $t_\omega \equiv e^{-i\frac{\omega}{v_c}\ell} - r^2 e^{+i\frac{\omega}{v_c}\ell}$ (and therefore $t_0 = 1 - r^2$). Equation (3) gives two equations which relate input, say $j_1(0)$ and $j_2(\ell)$, to output $j_1(\ell)$ and $j_2(0)$. All the coupled regions in a domain network is expressed by the form of equation (3). In the uncoupled region, the current density only acquires the phase like $e^{+i\frac{\omega}{v}\ell}$ since EMP propagates freely with the normal chirality. Therefore, current densities at the corners of the coupled regions can be eliminated for connected vertices, and the output current density is written as a function of the input current densities.

We numerically studied the transport properties in terms of the transmission probabilities observed at two detectors A and B, which are located at the lower left and upper right of the domain network, shown in figure 1(c) as an example, while the injection gate at the upper left gives an alternating current as an input. When each domain has EMPs with the chirality of the counterclockwise direction, we would expect that in the presence of an inter-domain interaction, the transmission signal of DetA is much larger than that of DetB if chirality of each domain is highly respected in a domain network.

4. Calculated results

Let us consider a square network that consists of regular octagons in which the length of each edge is ℓ. We use the units $\ell = v = 1$ and thus, the fundamental frequency of each domain is dimensionless, $\omega_0 = 2\pi/8$. The total length of the periphery of the 5×5 domains is 56ℓ, whose fundamental frequency is $\pi/28$. A small imaginary part of the frequency is included, i.e. $\omega \to \omega + \frac{i}{\tau}$, where we assume that $\tau = 500\ell/v$ to express the finite lifetime of excited states.

Figure 2(a) shows the calculated transmission spectrum for $r = 0.6$. The coupling constant is slightly larger than the highest value achieved using graphene so far ($r = 0.55$), [17] and we categorize it as a strong coupling because for $r \gtrsim 0.6$ the lowest energy eigenmode becomes the standing wave localizing in the coupled region [15].

A coherent wave with angular frequency ω is continuously excited at the injection gate of the upper left domain, and the transmissions to DetA at the lower left (T_A plotted as the blue curve) and DetB at the upper right (T_B plotted as the yellow curve) are plotted as a function of ω. Note that $1 - T_A - T_B$ is the signal

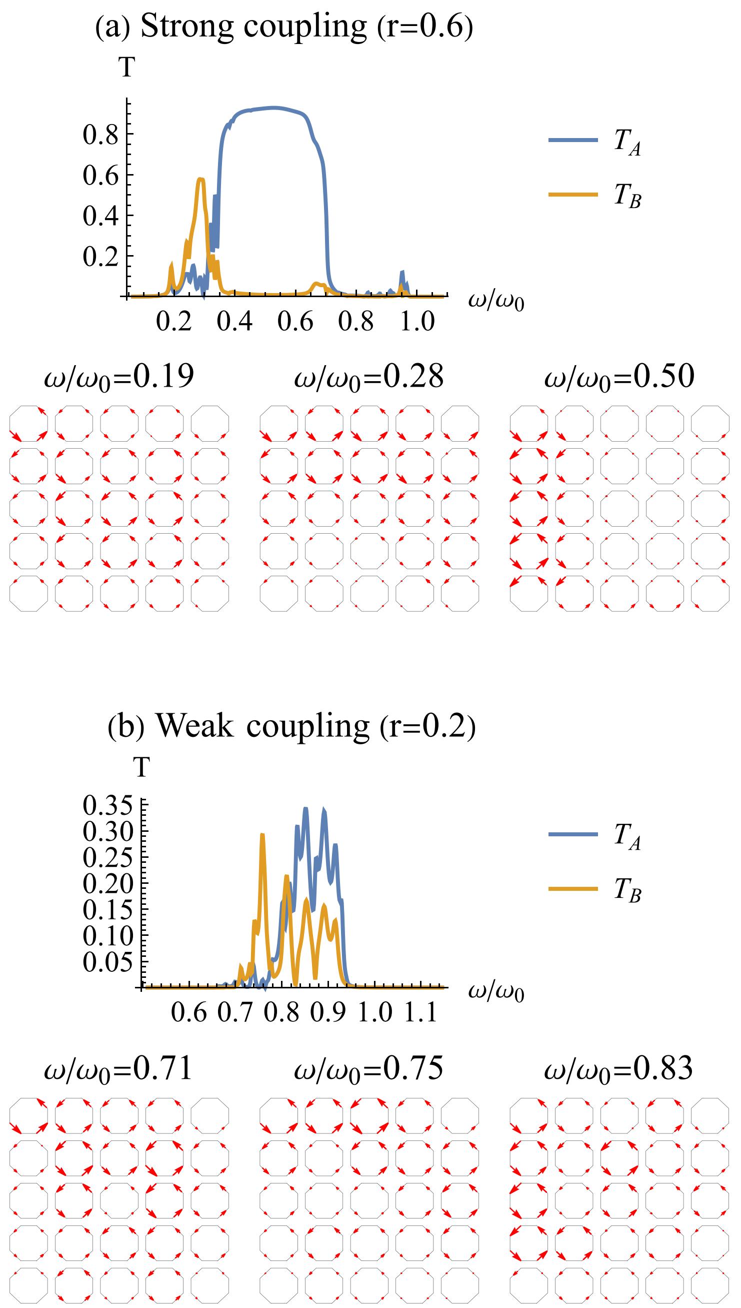

Figure 2. Transport properties of a square network. Results for a strong coupling constant, $r = 0.6$, (a) and weak coupling constant, $r = 0.2$, (b). (upper) Plots of transmission T_A (blue) and T_B (orange) as a function of ω/ω_0, where $\omega_0 = \pi v/4\ell$ is the fundamental frequency of the uncoupled octagonal domains. (lower) [left] Uniform current densities with small T_A and T_B mean non-chiral bulk transport. [center] A large T_B with small T_A means chirality reversal. [right] A large T_A with small T_B means chirality preservation.

strength at the output of the domain with the injection gate, which corresponds to the 'reflectance'. Each peak in the spectrum indicates an energy eigenmode of the system.

The spectrum can be divided into three regions from the viewpoint of chirality, namely, non-chirality, chirality reversal, and chirality preservation. These different transport properties appear in specific spectrum regions. First, the lowest spectral peaks of the network appearing at $\omega/\omega_0 = 0.19$ are an example of non-chirality. The peaks indicate $T_A \simeq T_B \ll 1$, and the vector plot of the current densities shows uniform propagation in bulk. Most of the energy inputted by the injection gate is 'reflected' at the domain. Next, the peaks at $\omega/\omega_0 = 0.28$ are an example of chirality reversal, for which $T_B \gg T_A$; the vector plot of the current densities shows the propagation along the edge, while its propagation direction is reversed from the chirality of the edge of outer domains. The macroscopic chirality of this mode is opposite to what would be naively expected from the chirality of the element. Finally, for the wide frequency range of $0.35 < \omega/\omega_0 < 0.7$, the edge channel with normal chirality appears in a macroscopic manner. From the corresponding band

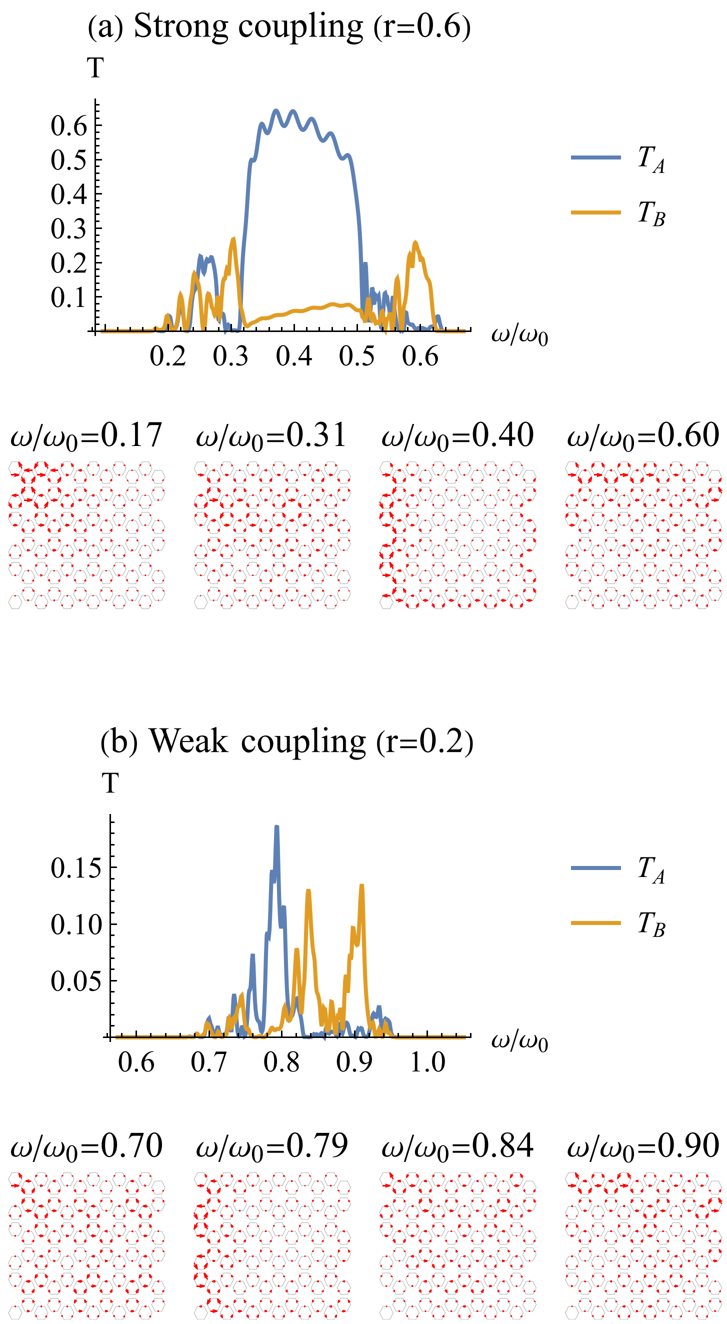

Figure 3. Transport properties of a honeycomb network. (a) Case of a strong-coupling constant. (upper) Plots of transmission T_A (blue) and T_B (orange) as a function of ω/ω_0, where $\omega_0 = \pi v/3\ell$ is the fundamental frequency of the hexagons. (lower) Vector plots of the three distinct phases; non-chiral bulk transport ($\omega/\omega_0 = 0.17$), chirality reversal($\omega/\omega_0 = 0.31$ and 0.6), and chirality preservation ($\omega/\omega_0 = 0.4$). (b) Case of a weak-coupling constant. $\omega/\omega_0 = 0.79$ is within the gap of the Dirac cone, and the edge channel with preserved chirality is clearly formed.

structure calculation [15], we can conclude that this frequency region is within the energy gap, suggesting a topological insulating phase of the system. For the cases of chirality reversal and preservation, the channels are localized at the periphery of the network and provide two-way edge transport at different frequencies.

Figure 2(b) depicts calculated results for a weak coupling, $r = 0.2$. For such a weak coupling, the values of T_A and T_B are at most 0.35, i.e. smaller than those for a strong coupling. The consequent small difference between T_A and T_B means that edge channels are not well formed, as shown in the vector plots, and rather that the wave extends into the bulk. Though it is difficult to get a general perspective on the transport in such a weakly coupled network, we consider that the transport tends to extend into the bulk in most cases. This conclusion does not change when the system size is increased from 5×5 to 10×10 domains.

Next, let us examine a network consisting of regular hexagons. Figure 3(a) shows the calculated transmission spectrum for $r = 0.6$. The results obtained for the strongly coupled honeycomb network bear some similarity to those of the strongly coupled square network, but some parts are in sharp contrast. First, within the energy gap covering a wide frequency range of $0.32 < \omega/\omega_0 < 0.5$, although chirality preservation is observed as $T_A \gg T_B$, which is similar to the square network, T_B is not close to zero. The edge channels continue to survive and reach DetB through DetA. Namely, the edge channel of the honeycomb network is more robust than the square network to the presence of the gate. The corresponding band structure calculation indicates that this frequency region is within the energy gap of the Dirac cone, [15] suggesting a sort of symmetry protection by which the edge channel with normal chirality appears in a macroscopic manner. Next, similarly to the square network, at both above and below of the energy gap ($\omega/\omega_0 = 0.31$ and 0.6), signals of chirality reversal ($T_B \gg T_A$) appear and the vector plot of the current densities corresponds to propagation along the edge, while its propagation direction is reversed from the chirality of the edge of outer domains. The lowest spectral peak of the network appearing at $\omega/\omega_0 = 0.17$ indicates non-chirality. The peaks show $T_A \simeq T_B \ll 1$, and the vector plot of the current densities shows uniform but still localized propagation in the bulk.

Figure 3(b) shows the results for a weak coupling honeycomb network with $r = 0.2$. T_A and T_B are each at most 0.2, which means that the edge channels are not well formed. There is a difference between T_A and T_B, but the wave extends into the bulk. Thus, for weakly coupled networks, we consider that transport tends to extend into the bulk in most cases. A unique exception is the formation of chiral edge channel at $\omega/\omega_0 = 0.79$, which is within the (small) energy band gap; it is well localized at the edge of the network.

5. Discussion and conclusion

As a general result for strongly-coupled domain networks, two-way edge channels formed at different energy levels. Within the energy gap, a one-way edge channel with normal chirality, that is, 'EMPs' with the same chirality character of elemental EMPs appear in a macroscopic scale, but below (or above) the gap, one-way edge channel with the reverse chirality exists. The origin of the energy gap of strongly-coupled domain networks is the inter-domain Coulomb interaction which can be related to the origin of the elemental EMPs. This suggests a possibility that there is some connection between the origins of the integer and fractional quantum Hall effects. Though it is popular that integer quantum Hall effect arises from the Landau quantization for non-interacting electrons in a strong magnetic field, there is an interesting viewpoint that the interaction of electrons is as important in the integer quantum Hall effect as in the fractional quantum Hall effect [20]. Namely, the former is the topological phase of interacting strongly correlated system at $\nu = 1$, similar to the latter with the difference in homotopy pattern for correlations specific to any particular fractional filling ratio from the fractional quantum Hall hierarchy.

In the vector plots of the current density, the current flow of the chirality reversal phase has large amplitudes not exactly at the outermost edges of the network but slightly inner from the outermost edges. This is in sharp contrast to the chirality preservation phase flowing at the outermost edges of the network. The difference in the flow paths of these edge channels is the main reason of that the peak height of T_B is not as large as that of T_A, since the both detectors are located at an outermost edge. Although the existence of chirality reversal, by itself, is intuitively clear in view of the charge fractionalization in the coupled region, it is not easy to understand how wave interference determines the details of the edge channels.

When the current amplitude is minimized to the level of a single electron, the quantum aspect of the network shows up, which is an interesting research subject. There are several theoretical methods to investigate the quantum phenomena of a network. Here we briefly mention one with a quantum field theoretical model. Indeed, for a two-domains system (1 and 2) having a coupled region, one-way edge channels (of uncoupled region) can be modeled by chiral liquids, [12, 21] while two-way channels (of coupled region) can be described by a TL liquid [22]. The Hamiltonian density of the total system takes the form,

$$H(x) = \frac{1}{2}\left(j_1(x) + j_2(x)\right)^2 + \frac{1}{2}\left(\frac{1-r(x)}{1+r(x)}\right)^2 \left(j_1(x) - j_2(x)\right)^2, \tag{5}$$

where $r(x)$ is the coupling constant, which is position dependent [15]. Where $r(x) = 0$ (i.e. in uncoupled regions), $j_1(x)$ and $j_2(x)$ are decoupled, while where $r(x) \neq 0$, the cross term of $j_1(x)j_2(x)$ remains. As a result, the coupled region can be described as a TL liquid with the parameter $K = (1-r)/(1+r)$ which determines the critical phenomena of the system. Thus, naively, there are two different vacuums (chiral and TL liquids) in the system. We expect for virtual-pair creations to occur near the boundary of the different vacuums, which are quantum fluctuations or a quantum mechanical version of the charge fractionalization phenomena (see figures 1(a) and (b)).

To conclude, in order to establish mutual telecommunication through edge channels between two detectors located at outermost domains in a network, excitations with different frequencies are necessary.

The energy levels of the two edge channels are within the gap or below (or above) it. The detectors having output channels also have input channels that affect the current flow, whose effect depends on the network shape. The numerical program developed in this study is readily applicable to arbitrary shape of domain network with additional gate electrodes for input and detection. Thus, it may be useful in the analysis of experimental results.

Data availability statement

All data that support the findings of this study are included within the article (and any supplementary files).

Acknowledgment

The author thanks M Hashisaka and K Muraki. The author thanks N Kumada for discussions and for sharing a figure.

ORCID iD

Ken-ichi Sasaki https://orcid.org/0000-0002-0658-4911

References

[1] Kohmoto M 1985 Topological invariant and the quantization of the Hall conductance *Ann. Phys., NY* **160** 343–54
[2] Kane C L and Mele E J 2005 Z2 topological order and the quantum spin hall effect *Phys. Rev. Lett.* **95** 146802
[3] Halperin B I 1982 Quantized Hall conductance, current-carrying edge states and the existence of extended states in a two-dimensional disordered potential *Phys. Rev.* B **25** 2185–90
[4] Allen S J, Störmer H L and Hwang J C M 1983 Dimensional resonance of the two-dimensional electron gas in selectively doped GaAs/AlGaAs heterostructures *Phys. Rev.* B **28** 4875–7
[5] Mast D B, Dahm A J and Fetter A L 1985 Observation of bulk and edge magnetoplasmons in a two-dimensional electron fluid *Phys. Rev. Lett.* **54** 1706–9
[6] Glattli D C, Andrei E Y, Deville G, Poitrenaud J and Williams F I B 1985 Dynamical hall effect in a two-dimensional classical plasma *Phys. Rev. Lett.* **54** 1710–3
[7] Volkov V A and Mikhailov S A 1988 Edge magnetoplasmons: low-frequency weakly damped excitations in inhomogeneous two-dimensional electron systems *Sov. Phys. JETP* **67** 1639
[8] Sasaki K-ichi, Murakami S, Tokura Y and Yamamoto H 2016 Determination of intrinsic lifetime of edge magnetoplasmons *Phys. Rev.* B **93** 125402
[9] Jin D, Christensen T, Soljačić M, Fang N X, Ling L and Zhang X 2017 Infrared topological plasmons in graphene *Phys. Rev. Lett.* **118** 245301
[10] MacDonald A H 1990 Edge states in the fractional-quantum-Hall-effect regime *Phys. Rev. Lett.* **64** 220–3
[11] Wassermeier M, Oshinowo J, Kotthaus J P, MacDonald A H, Foxon C T and Harris J J 1990 Edge magnetoplasmons in the fractional-quantum-Hall-effect regime *Phys. Rev.* B **41** 10287–90
[12] Wen X G 1990a Electrodynamical properties of gapless edge excitations in the fractional quantum Hall states *Phys. Rev. Lett.* **64** 2206–9
[13] Kane C L and Mele E J 2005b Quantum spin hall effect in graphene *Phys. Rev. Lett.* **95** 226801
[14] Hashisaka M and Fujisawa T 2018 Tomonaga–Luttinger-liquid nature of edge excitations in integer quantum Hall edge channels *Rev. Phys.* **3** 32–43
[15] Sasaki K-I 2022 Band structures of edge magnetoplasmon crystals *Phys. Rev.* B **105** 075312
[16] Kamata H, Kumada N, Hashisaka M, Muraki K and Fujisawa T 2014 Fractionalized wave packets from an artificial Tomonaga–Luttinger liquid *Nat. Nanotechnol.* **9** 177–81
[17] Brasseur P, Ngoc Han T, Sekine Y, Muraki K, Hashisaka M, Fujisawa T and Kumada N 2017 Charge fractionalization in artificial Tomonaga-Luttinger liquids with controlled interaction strength *Phys. Rev.* B **96** 081101
[18] Scholl J A, García-Etxarri A, Leen Koh A and Dionne J A 2013 Observation of quantum tunneling between two plasmonic nanoparticles *Nano Lett.* **13** 564–9
[19] Hashisaka M, Kamata H, Kumada N, Washio K, Murata R, Muraki K and Fujisawa T 2013 Distributed-element circuit model of edge magnetoplasmon transport *Phys. Rev.* B **88** 235409
[20] Jacak J E 2021 Topological approach to electron correlations at fractional quantum Hall effect *Ann. Phys., NY* **430** 168493
[21] Wen X G 1990b Chiral Luttinger liquid and the edge excitations in the fractional quantum Hall states *Phys. Rev.* B **41** 12838–44
[22] Tomonaga S-I 1950 Remarks on Bloch's method of sound waves applied to many-fermion problems *Prog. Theor. Phys.* **5** 544